flow rate and the filtration pressure was observed in our system. It is assumed that the pores in the membranes are cylinders with a constant mean radius. The cylindrical pores form a statistical, three-dimensional network in the membrane. Thus, the mean pore radius, r, includes the tortuous factors:

$$J = n'\pi r^4 \Delta P/8\mu L \quad (5)$$

where n', μ, and ΔP are the pore number of effective surface area, viscosity, and the filtration pressure, respectively. Inserting eqs 2 and 4 into eq 5 yields

$$J = 2n'\{v_p - (v + W_0 G v_a - V)\}^2 \Delta P/\mu n^2 \pi^3 D^4 L^3 \quad (6)$$

Since the dimensions and the flux of the membrane were measured as shown in Figures 2 and 3, respectively, the apparent specific volume of the graft phase can be obtained as a function of the degree of grafting. The grafted polymer branches are formed in two domains of the porous CTA membrane: the pore surface and the amorphous domain in the matrix. The apparent specific volume of the graft phase is defined by (the volume of the graft phase which is assumed to be formed exclusively on the pore surface)/(the weight increase calculated from the degree of grafting). Therefore, the higher volume ratio of the graft phase on the pore surface yields a higher value for v_a. On the contrary, when most of the graft phase is formed in the amorphous domain of the matrix, v_a approaches zero.

As shown in Figure 4, the v_a for the V-MMA-CTA membrane increased with an increasing degree of grafting, whereas the value of v_a for the L-MMA-CTA membrane slightly increased until the degree of grafting was 30% and approximately leveled off at about 1.5 cm^3/g. These results indicated that the grafted branches are located in the amorphous region of the trunk polymer in vapor-phase grafting but in the pore surface in liquid-phase grafting at a lower degree of grafting.

Morphological Change of Pore Structure. SEM photographs of the surfaces of the starting, V-MMA-CTA, and L-MMA-CTA membranes are shown in Figure 5. The reduction in porosity of the MMA-grafted membranes was observed in comparison with the starting membrane. The above discussion of the location of the grafted branches agreed fairly well with the morphology of the surfaces of the membranes whose degree of grafting were 25 and 60%. As shown in Figure 5b, the white part, indicating the CTA-MMA graft copolymer network, swelled in the L-MMA-CTA membrane due to the formation of grafted branches on the pore surface. Also, the pore diameter decreased with an increasing degree of grafting. In contrast, Figure 5c shows that the porous structure of the V-MMA-CTA membrane was almost identical with that of the starting membrane even with an increasing degree of grafting. The graft chains prepared by vapor-phase grafting entered the amorphous domain in the trunk polymer and allowed the volume of the membrane to increase, as also shown in Figure 2c.

(6) Morita, Z.; Ishida, H.; Shimamoto, H.; Weber, R.; Rys, P. *J. Membr. Sci.* **1989**, *46*, 283.

Notation

D	diameter of MMA-grafted flat membrane, m
G	dimensionless degree of grafting
J	pure water flux, $m^3/(m^2\ h)$
L	thickness of MMA-grafted membrane, m
n	number of pores per surface area of membrane, m^{-2}
n'	number of pores per effective surface area of membrane, m^{-2}
ΔP	filtration pressure, Pa
r	mean pore radius of MMA-grafted membrane, m
v	volume of starting membrane (including pore volume), m^3
v_a	apparent specific volume of graft phase, m^3/kg
v_p	pore volume of starting flat membrane, m^3
V	volume of MMA-grafted membrane (including pore volume), m^3
ΔV_p	pore volume filled by grafted branches, m^3
W_0	weight of starting membrane, kg
W_1	weight of MMA-grafted membrane, kg
μ	viscosity, Pa h

Acknowledgment. Helpful discussions with Min Kim are gratefully acknowledged. We are also grafteful to Hiroshi Ito of the Japan Atomic Energy Research Institute for performing the SEM measurements.

Alkali-Metal-Free Carbonate Coprecipitation: An Effective Synthetic Route to Bismuth-Based Oxide Superconductors

Nicholas D. Spencer

W. R. Grace & Co.-Conn., Research Division, 7379 Route 32, Columbia, Maryland 21044

Received May 30, 1990

Bismuth lead strontium calcium copper oxide superconductors are conveniently synthesized via coprecipitation by means of a tetraalkylammonium carbonate. This technique has the advantage over solid-state methods of placing the metal ions in close proximity prior to calcination. Precipitation pH has been optimized by monitoring its effect on metal concentrations in the filtrate, crystallinity of the precipitate, filtering times, and properties of the calcined, superconducting material. The sample initially precipitated at pH 8 produces the most phase-pure ~2223 material.

Introduction

Coprecipitation of oxide precursors such as hydroxides or carbonates is a widely used technique in the synthesis of many mixed metal oxides.[1] It has the significant advantage over solid-state synthesis ("grind-and-fire" methods) of potentially placing the component metal ions within atomic distances of each other, greatly facilitating solid-state diffusion and minimizing the risk of unwanted phase formation. Furthermore, coprecipitation avoids the grinding steps inherent in solid-state synthesis, which can ultimately lower phase purity by the incorporation of grinding media. Complications arise, however, when the conditions for precipitation of the individual component

(1) Johnson, D. W.; Gallagher, P. K.; Schrey, F.; Rhodes, W. W. *Ceram. Bull.* **1976**, *55*, 520-527.

0897-4756/90/2802-0708$02.50/0

hydroxides or carbonates are significantly different. In the case of the Y–Ba–Cu–O and Bi–Ca–Sr–Cu–O superconductor systems, for example, hydroxide coprecipitation is not a viable option, due to the significant solubility of Ca, Sr, and Ba hydroxides. Carbonate coprecipitation of the Y–Ba–Cu–O system has been described by Wang et al.[2], who used potassium carbonate as a precipitating agent. This method does present a potential problem, however, in that residual potassium is difficult to eliminate from the precipitate, even with extensive washing. Washing, itself, causes problems also, since Ba, Sr, and Ca carbonates are all slightly water soluble at room temperature (0.001–0.002 g/100 cm^3). In electronic applications in particular, traces of alkali-metal impurities are highly undesirable.

Ammonium carbonate is often used as a precipitating agent in catalyst preparation, since the cation can readily be removed by thermal treatment. In copper-containing systems, however, there is an added complication, since these metal ions form highly soluble ammine complexes. Reducing the pH can, in principle, solve this problem but leads to the formation of the bicarbonate rather than the carbonate ion. In the Y–Ba–Cu–O and Bi–Ca–Sr–Cu–O systems, this presents another problem, since group 2 bicarbonates have significant solubility at room temperature.

The precipitating agent used in the present study is tetramethylammonium carbonate (TMA_2CO_3). As with ammonium carbonate, the cation can be thermally decomposed, but unlike the ammonium ion, $N(CH_3)_4^+$ does not readily form a neutral species that can be complexed by copper. Thus, an intimate mixture of carbonates and hydroxycarbonates can be precipitated with TMA_2CO_3, which after drying and calcination forms a mixed oxide powder containing neither impurities from the precipitation nor impurities from the grinding media. This method has been described, as applied to the Y–Ba–Cu system, by Spencer et al.[3] and Bunker et al.[4]

This paper deals with some aspects of the solution chemistry involved in the TMA_2CO_3 precipitation of the Bi–Pb–Ca–Sr–Cu–O system and its impact on the superconducting materials formed by subsequent calcination.

Experimental Section

An aqueous stock solution containing bismuth, lead, strontium, calcium, and copper nitrates was prepared, with additional nitric acid being used to facilitate dissolution of the bismuth component. The metals were in the correct stoichiometric ratio to form $Bi_{1.8}Pb_{0.2}Ca_2Sr_2Cu_3O_{10}$ (–2223), with a copper molarity of 0.1. All nitrates were of at least 99.9% purity (Aldrich Chemical Co.). Aqueous tetramethylammonium (TMA) hydroxide solution (25 wt %, Southwestern Analytical Chemicals) was carbonated with CO_2 until the pH was 10.0. It was then diluted with deionized water to make a 0.58 M TMA_2CO_3 solution.

The metals solution and the TMA_2CO_3 solution were simultaneously dripped, at identical flow rates, into a third equal volume of deionized water, while stirring vigorously. The pH was held constant by means of a stream of neat (25 wt %) TMA hydroxide. The precipitation was carried out over 30 min, after which the slurry was stirred for a further 30 min and filtered over a double thickness of Whatman No. 5 filter paper. The filter cake was not washed. The filtration process was timed, and the filtrate analyzed for metals by inductively coupled plasma (ICP) atomic emission spectroscopy. The filter cake was dried for 16 h at 110 °C in air. This material was then heated to 540 °C for 5 h in air to decompose any remaining TMA. Further calcination was carried out for 12 h at 800 °C in air, from which CO_2 had been removed by an Ascarite scrubber. This powder was then pressed into 3-g $^1/_2$-in.-diameter pellets with 5000 lbf and heated in air for 60 h at 860 °C, followed by cooling over 8 h to 350 °C and then rapidly cooling to room temperature. After these pellets were ground and characterized, they were repelletized and reheated in air for 96 h at 870 °C, again followed by cooling over 8 h to 350 °C and then rapidly cooling to room temperature.

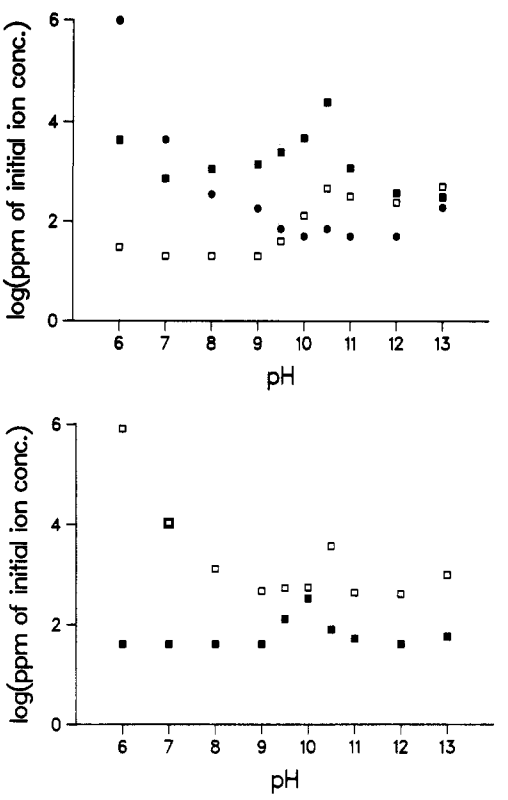

Figure 1. Filtrate concentrations of metal ions following precipitation step: (top) Cu (■), Pb (□), and Sr (●); (bottom) Bi (■) and Ca (□).

X-ray diffraction patterns were obtained for the materials produced after all drying and heating steps. Scanning electron micrographs were obtained after the 540 °C calcination. The 860 and 870 °C calcined pellets were crushed and evaluated by ac magnetic susceptibility. The entire precipitation, filtration, drying, and calcination sequence was repeated 10 times at pH 6, 7, 8, 9, 9.5, 10, 10.5, 11, 12, and 13 using TMA_2CO_3/TMAOH, as well as once at pH = 10.5 using K_2CO_3/KOH.

The X-ray diffraction equipment consisted of a Philips APD 3600 diffractometer (graphite monochromator and θ-compensating slits) using Cu Kα radiation and a scan rate of 2° 2θ min^{-1}. Scanning electron micrographs were taken on a Hitachi Model 5570 instrument with a 20-kV electron beam energy. Ac magnetic susceptibility data were obtained by using a Quantum Technology Corp. Meissner probe operating at 20 kHz and a maximum ac field of 1 Oe. Particle-size data were obtained by a laser-light-scattering technique (Malvern MasterSizer). Samples were suspended in decane containing a 5 wt % concentration of Oloa 1200 (Chevron Chemicals) as a dispersing agent[5] and were sonicated for 30 min at medium power prior to measurement.

Results and Discussion

The top and bottom parts of Figure 1 show the variation in the filtrate concentrations[6] of Cu, Pb, and Sr and Bi and

(2) Wang, H. H.; Carlson, K. D.; Geiser, U.; Thorn, R. J.; Kao, H.-L. I.; Beno, M. A.; Monaghan, M. R.; Allen, T. J.; Proksch, R. B.; Stupka, D. L.; Williams, J. M.; Flandermeyer, B. K.; Poeppel, R. B. *Inorg. Chem.* 1987, *26*, 1476–1481.

(3) Spencer, N. D.; Pan, W. H.; Rudesill, J. A. European Patent Application 0306973, 1988.

(4) Bunker, B. C.; Voight, J. A.; Lamppa, D. L.; Doughty, D. H.; Venturini, E. L.; Kwak, F. J.; Ginley, D. S.; Headley, T. J.; Harrington, M. S.; Eatough, M. O.; Tissot, R. G.; Hammetter, W. F. In *Better Ceramics Through Chemistry*; Brinker, C. J., Clark, D. E., Ulrich, D. R., Eds.; MRS Symposium Proceedings 121; Materials Research Society: Pittsburgh, PA, 1988; Vol. III, pp 373–384.

(5) Dolhert, L. E., W. R. Grace & Co.-Conn., Research Division, personal communication, 1989.

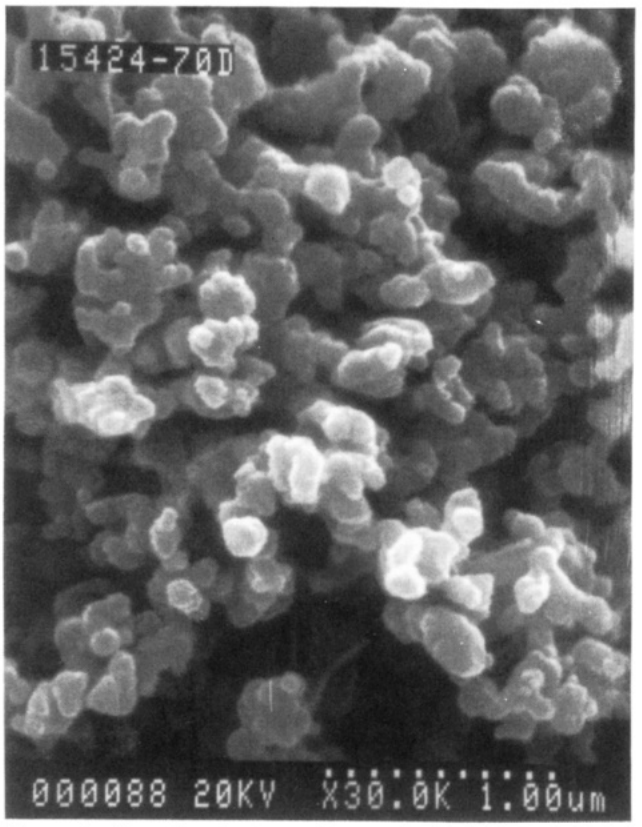

Figure 2. Scanning electron micrograph of pH 8 precipitated material following 540 °C heating step.

Ca, respectively, as a function of precipitation pH. The most significant filtrate concentrations are to be found at low pH and in the region pH 10–11. At pH 6–7, very high concentrations of calcium and strontium were detected, presumably due to the formation of the soluble bicarbonates. The copper maximum at pH 10.5 is at first sight surprising, since the solubilities of copper hydroxide and copper carbonate are both near their minimum values at this pH.[7] There is, however, a major perturbation introduced by the presence of a small but significant concentration of the free trimethylamine, formed by the decomposition of the TMA^+ cation. This is detectable by its characteristic fishy odor. N-containing ligands, such as ammonia, are known to introduce characteristic maxima in copper solubility in the pH 9–11 region,[7] and trimethylamine would be expected to behave in a very similar way. In a control experiment using K_2CO_3/KOH (i.e., in the absence of any complexing agents), the copper concentration in the filtrate from a pH 10.5 precipitation was 56 ppm[6]—nearly 3 orders of magnitude lower than in the equivalent TMA experiment.

The maximum copper concentration in the filtrate corresponds to approximately 2% of the copper originally present in the metals solution. This would represent an unacceptable deviation from the desired stoichiometry in the finished material. At pH 6, virtually all of the calcium and strontium present in the starting solution are carried through into the filtrate. From a solubility standpoint, the ideal pH values appear to be around 8 and around 12.

Precipitate particle size is often strongly dependent on pH, but in this case, SEM pictures of the material, once

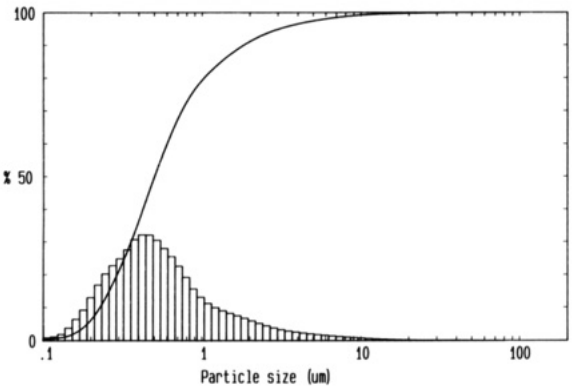

Figure 3. Particle-size distribution of pH 8 precipitated material following 540 °C heating step.

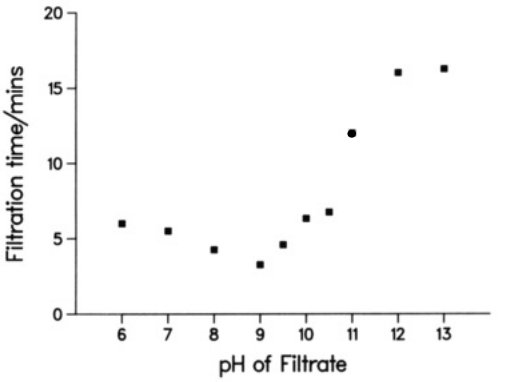

Figure 4. Filtering time of precipitate slurry as a function of precipitation pH.

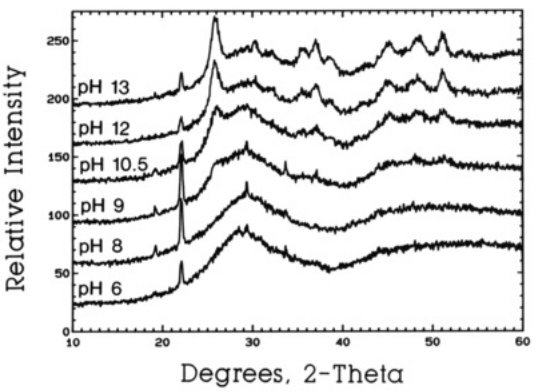

Figure 5. X-ray diffraction patterns of precipitates formed at pH 6, 8, 9, 10.5, 12, and 13, following drying at 110 °C.

it had been heated to 540 °C to remove organics, showed very similar morphologies in all samples (Figure 2). Particle size appeared in SEM to be in the 0.1–0.2-μm range, although light-scattering data (Figure 3) suggest that these are agglomerated to a mean size of 0.4–0.5 μm.

Filtering time showed a dramatic pH dependence (Figure 4), increasing more than 5-fold between pH 9 and pH 12.[8] This is presumably due to the steadily increasing negative charge on the precipitate particles as pH is increased, leading to increased interparticle repulsion and a reduction in agglomeration. At pH 12 or 13 the agglomerates in the slurry are probably of dimensions comparable to the filter-paper pores (2.5 μm for Whatman No.

(6) Expressed as ppm of the initial ion concentrations in the metal nitrate solution, corrected for the dilution occurring during the precipitation process.

(7) Kragten, J. *Atlas of Metal-Ligand Equilibria in Aqueous Solution*; Wiley: New York, 1978.

(8) Clearly, absolute filtering times depend on the amount of material, pressure drop across the filter paper, and size of filtering equipment. The actual times are given rather than arbitrary units to present an approximate guide under "typical" lab conditions at the 0.017 mole preparatory scale.

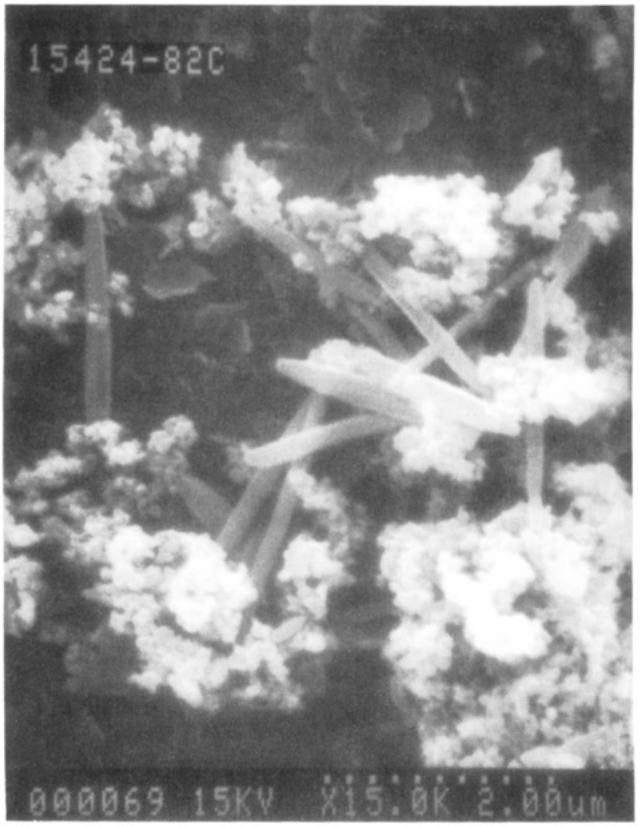

Figure 6. Scanning electron micrograph of pH 6 precipitated material following drying at 110 °C.

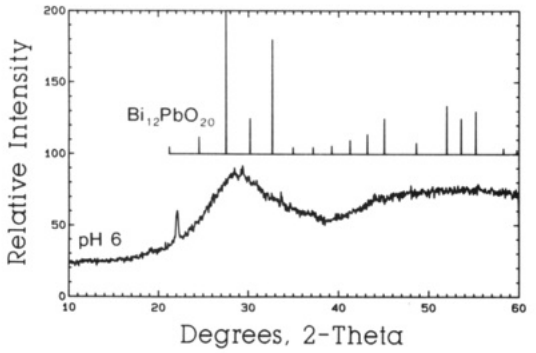

Figure 7. X-ray diffraction pattern of pH 6 precipitated material following drying at 110 °C, compared with library pattern for $Bi_{12}PbO_{20}$.

5), and lead to clogging, whereas at pH 8 or 9 the particles are much more agglomerated and do not enter the filter pores. This means that of the two solubility minima at pH 8 and 12, the former is to be preferred on practical grounds, since filtration can be performed more rapidly.

Another reason to favor pH 8 can be seen in the XRD patterns of the dried precipitate (Figure 5). At pH 6, the pattern is generally amorphous, with sharp peaks at $2\theta \approx 22°$ and 29.5°. SEM of this material (Figure 6) reveals needlelike crystals amid small-particle-size material, in perfect accord with the XRD observations. A water wash of the precipitate (usually not undertaken, in an effort to preserve metal stoichiometry) leads to an XRD pattern totally devoid of the sharp peaks. This strongly suggests that they are due to remaining $TMANO_3$. This would also account for the disappearance of these peaks on subsequent heating to 540 °C (see below). The amorphous envelope correlates well with $Bi_{12}PbO_{20}$ (Figure 7). All features present at pH 6 are also to be seen at other pH values, but as the pH increases, other unidentified crystalline phases appear. The peak widths of the high-pH features correspond to a crystallite size of a few hundred angstroms. Thus, pH 8 is more amorphous than pH 12, suggesting greater homogeneity, which is clearly desirable from the standpoint of ultimate phase purity. However, even at the higher pH, the crystallite sizes are much smaller than the 0.1–0.5-μm particle size of the 540 °C calcined superconductor precursor. The large number of unidentified peaks in the precipitate is a consequence of the complexity of the system, which contains Bi^{3+}, Pb^{2+}, Ca^{2+}, Sr^{2+}, Cu^{2+}, TMA^+, CO_3^{2-}, OH^-, NO_3^-, and probably O^{2-} as well, some of which may be in solid solution.

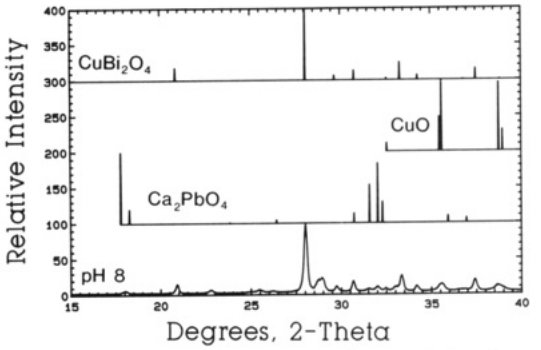

Figure 8. X-ray diffraction pattern of pH 8 precipitated material following heating at 540 °C, compared with library patterns for Ca_2PbO_4, CuO, and $CuBi_2O_4$.

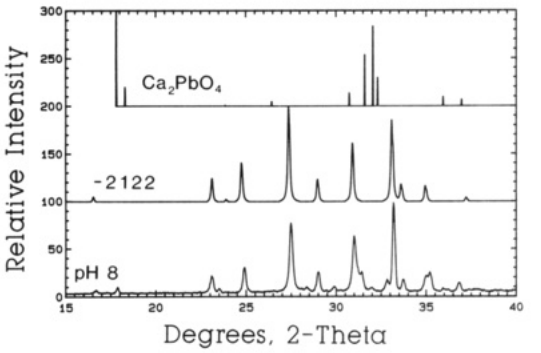

Figure 9. X-ray diffraction pattern of pH 8 precipitated material following heating at 800 °C, compared with library patterns for Ca_2PbO_4 and -2122.

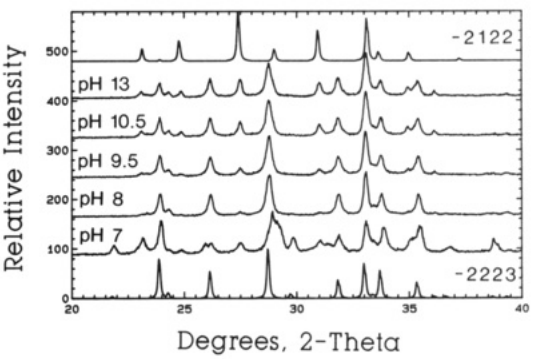

Figure 10. X-ray diffraction patterns of materials precipitated at pH 7, 8, 9.5, 10.5, and 13 following heating at 860 and 870 °C, compared with library patterns for -2122 and -2223 phases.

After the 540 °C calcination, there is little variation between the XRD patterns of materials prepared at different pH values. Figure 8 shows the XRD pattern of the pH 8 sample, and most peaks may be identified as corresponding to CuO, $CuBi_2O_4$, and Ca_2PbO_4.

On heating to 800 °C, the (Ca- and Sr-deficient) pH 6 sample melted. XRD patterns of all other samples display

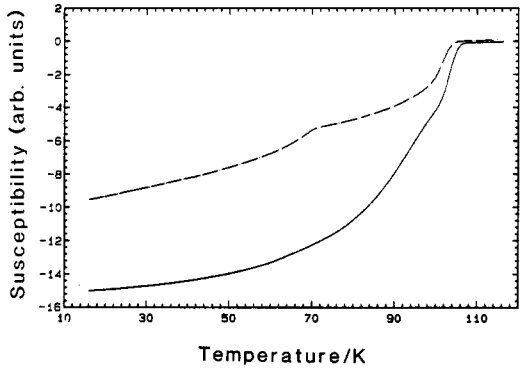

Figure 11. Ac susceptibility measurements of materials precipitated at pH 7 (dashed) and 8 (solid), following heating at 860 and 870 °C.

peaks characteristic of $Bi_{1-x}Pb_xCaSr_2Cu_2O_8$ (-2122) and show little pH dependence (Figure 9). Other peaks are mostly attributable to Ca_2PbO_4.

After the heatings at 860 °C, all samples showed roughly equal amounts of the -2122 and -2223 phases. However, following the 870 °C treatment, clear differences and trends are to be seen in the XRD patterns (Figure 10). The pH 7 sample shows a mixture of comparable amounts of the -2122 and -2223 phases. Since we saw (Figure 1, bottom) a substantial loss of Ca at this pH, this is not surprising, since there is a greater requirement for Ca (sandwiched between the CuO sheets) in the -2223 form. The pH 8 pattern shows nearly single-phase -2223, and this is confirmed in ac susceptibility measurements (Figure 11), where only a slight deviation from the single transition at 107 K is to be seen. This is in marked contrast to the clear double transition observed for the pH 7 sample. The XRD pattern for pH 9 is very similar to that of pH 8. As the pH is increased further, however, the concentration of the -2122 phase steadily increases (Figure 10). This may be due to the increased lead loss above pH 9 (Figure 1, top), since lead is a well-known promoter of the -2122 to -2223 reaction.[9,10]

Summary and Conclusions

TMA_2CO_3/TMAOH precipitation of precursors to the Bi-Pb-Ca-Sr-Cu-O system is an efficient method of placing the metal ions in intimate contact with each other prior to calcination. Precise stoichiometric control can be maintained, provided that the pH is held at around 8 or 12 during the entire precipitation. pH 8 is preferable, since pH 12 leads to larger crystallites, which reduce homogeneity, and smaller agglomerates, which extend filtering times.

With the exception of the material formed at pH 6, which was extremely deficient in Ca and Sr and melted at <800 °C, all precipitates ultimately formed a mixture of the -2122 and -2223 structures when calcined first at 800 °C and then at 860 and 870 °C. The sample initially precipitated at pH 8 seems to produce the most phase-pure -2223 material.

Acknowledgment. I am very grateful to Ted Peders for his skillful sample preparation and to Jane Swain, Bob Collins, and Eric Taylor for their analytical assistance.

Registry No. $Bi_{1.8}Pb_{0.2}Sr_2Ca_2Cu_3O_{10}$, 118903-34-7; tetramethylammonium carbonate, 40105-52-0.

(9) Takano, M.; Takada, J.; Oda, K.; Kitaguchi, H.; Miura, Y.; Ikeda, Y.; Tomii, Y.; Mazaki, H. *Jpn. J. Appl. Phys.* **1988**, *27*, L1041-L1043.
(10) Green, S. M.; Jiang, C.; Mei, Y.; Luo, H. L.; Politis, C. *Phys. Rev. B* **1988**, *38*, 5016-5018.

Growth of Zeolite Crystallites and Coatings on Metal Surfaces

Shawn P. Davis,[†,‡] Eric V. R. Borgstedt,[‡] and Steven L. Suib*[,†,‡,§]

Department of Chemistry, Institute of Materials Science, and Department of Chemical Engineering, U-60, University of Connecticut, Storrs, Connecticut 06269-3060

Received May 11, 1990

Zeolite crystals have been grown on metal surfaces by modified hydrothermal alteration methods. Coatings of zeolites can be grown in thicknesses ranging from 1 μm to about 1 mm. Zeolite crystals can be selectively bonded to one side of the metal substrate due to gravitational effects during the zeolite crystallization. Several types of syntheses have been successful, such as the growth of crystals at metal surfaces directly in the autoclave and growth of zeolites at metal surfaces that have been spin coated or immersed in various mother liquors. The zeolites have been characterized by X-ray powder diffraction, scanning electron microscopy, luminescence spectroscopy, 180° peel strength measurements, and surface area measurements. Details of the synthetic preparation are also discussed. The purpose of making such coatings is to prepare new materials with possible uses in such areas as electrochemistry, catalysis, adsorption, sensor applications, semiconductor circuitry, and photochemistry.

I. Introduction

Thin films are typically composed of metals or semiconductors.[1] Preparative methods of thin films include vapor deposition, radio frequency sputtering, and laser beam deposition.[2] The thickness of films can be monitored in a variety of ways including piezoelectric quartz crystals, X-ray fluorescence, eddy current measurements,

Table I. Scotch Tape 180° Peel Strength Measurements (51 mm/min) of Various Thicknesses of Zeolite Coatings on Copper Foil (Values in g/mm)

sample	first trial	second trial
thick zeolite coating (1 mm)	1	24
intermediate zeolite coating (<0.5 mm)	18	47
thin zeolite coating (<0.5 mm), Eu^{3+} exchanged	32	38

[†] Department of Chemistry.
[‡] Institute of Materials Science.
[§] Department of Chemical Engineering.
* To whom correspondence should be addressed at the Department of Chemistry.

0897-4756/90/2802-0712$02.50/0